ACCEPTED MANUSCRIPT

6 μm thick AlInP ^{55}Fe X-ray photovoltaic and ^{63}Ni betavoltaic cells

6 μm thick AlInP ^{55}Fe X-ray photovoltaic and ^{63}Ni betavoltaic cells

S Butera[1,*], M D C Whitaker[1], A B Krysa[2], A M Barnett[1]

[1]Space Research Group, School of Engineering and Informatics, University of Sussex, Brighton, BN1 9QT, UK.

[2]EPSRC National Epitaxy Facility, University of Sheffield, Mappin Street, Sheffield, S1 3JD, UK.

*Corresponding author. Electronic mail: S.Butera@sussex.ac.uk.

Abstract. Two 400 μm diameter $Al_{0.52}In_{0.48}P$ p^+-i-n^+ mesa photodiodes (6 μm i layer) were fabricated from a wafer grown by metalorganic vapour phase epitaxy (MOVPE) and then studied at temperatures from 140 °C to -20 °C for the development of temperature tolerant ^{55}Fe X-ray photovoltaic and ^{63}Ni betavoltaic microbatteries. The $Al_{0.52}In_{0.48}P$ epitaxial layers are the thickest so far reported for this emerging application. At each temperature, the performances of the $Al_{0.52}In_{0.48}P$ detectors were analysed in dark conditions, as well as under the illumination of a 182 MBq ^{55}Fe radioisotope X-ray source and a 185 MBq ^{63}Ni radioisotope source. An open circuit voltage as high as 1.13 V was found for both the $Al_{0.52}In_{0.48}P$ X-ray photovoltaic cells at -20 °C; whilst an open circuit voltage of 0.47 V was found for the best ^{63}Ni betavoltaic cell, at the same temperature. Maximum output powers of 1.44 pW and 1.36 pW were obtained from the two X-ray photovoltaic cells at -20 °C; combining the output powers of these two $Al_{0.52}In_{0.48}P$ X-ray photovoltaic cells, a total maximum output power as high as 2.8 pW could be obtained at -20 °C. Maximum output powers of 0.18 pW and 0.13 pW were instead extracted from the two betavoltaic cells at -20 °C, these could lead to a total maximum output power as high as 0.3 pW at -20 °C. Conversion efficiencies of 2.2% and 0.06% were found, respectively, for the best $Al_{0.52}In_{0.48}P$ X-ray photovoltaic and betavoltaic cells at -20 °C. With respect to previously reported $Al_{0.52}In_{0.48}P$ X-ray photovoltaic cells with thinner i layers, the 6 μm $Al_{0.52}In_{0.48}P$ X-ray photovoltaic cells had higher short circuit current, open circuit voltage, maximum output power, and conversion efficiency. The 6 μm $Al_{0.52}In_{0.48}P$ betavoltaic cells instead presented similar performances to previously analysed $Al_{0.52}In_{0.48}P$ betavoltaic cells.

Keywords: AlInP, photovoltaic and betavoltaic cells, semiconductors

1

1. INTRODUCTION

In recent years, $Al_{0.52}In_{0.48}P$ has been used in a variety of applications including, laser diodes [1], solar cells [2], and underwater communication systems [3]. Lately, it has also attracted research attention for its use in direct conversion nuclear microbatteries, which convert the energy released during decay of a radioisotope into electrical energy. Such nuclear microbatteries can be beneficial for many long life applications including microelectromechanical system technologies [4], biomedical uses [5], and aerospace applications [6]. A problem with direct conversion microbatteries is that the emissions from the radioactive source can damage the semiconductor converter layer; a material that may overcome this radiation damage problem is $Al_{0.52}In_{0.48}P$. Recently, the first $Al_{0.52}In_{0.48}P$ X-ray photovoltaic [7] and betavoltaic [8] cells have been reported. These initial devices were shown to have open circuit voltages of 0.97 V and 0.52 V, and maximum output powers of 0.62 pW and 0.28 pW at -20 °C, respectively [7, 8]. Those X-ray photovoltaic and betavoltaic cells both used 2 μm i layer $Al_{0.52}In_{0.48}P$ detectors as the converter devices; which were the thickest $Al_{0.52}In_{0.48}P$ epitaxial layers reported at the time. Other characteristics that make $Al_{0.52}In_{0.48}P$ converter layers desirable in a nuclear microbattery include its wide bandgap (2.31 eV [3]) and its high linear attenuation coefficients. The wide bandgap of $Al_{0.52}In_{0.48}P$ should result, unlike Si, Ge, and other narrower bandgap materials, in a high microbattery conversion efficiency [9, 10] as well as low thermally-generated leakage currents [7, 8] even at increased working temperatures. The large $Al_{0.52}In_{0.48}P$ linear attenuation coefficients mean that thinner $Al_{0.52}In_{0.48}P$ photodiodes can achieve the same detection efficiency as thicker detectors made from other materials with lower attenuation coefficients (e.g. Si, GaAs, AlGaAs). Moreover, $Al_{0.52}In_{0.48}P$ has the advantage of being very nearly lattice matched with commercially available GaAs substrates, which can facilitate its scientific exploitation and commercial production.

All these properties make $Al_{0.52}In_{0.48}P$ a promising candidate material for high-efficiency, high-energy-density, and temperature-tolerant nuclear microbatteries. Other wide bandgap detector technologies for nuclear microbatteries include GaAs [11, 12, 13], SiC [10, 14], AlGaAs [15, 16], InGaP [17, 18, 19, 20], GaN [21, 22], and diamond [23]. X-ray, beta, and alpha radioisotope sources have been coupled to such semiconductor materials to achieve the conversion of nuclear energy into electrical energy. The use of a radioisotope X-ray source (e.g. [55]Fe) or a radioisotope beta particle source (e.g. [63]Ni) rather than a radioisotope alpha source can be advantageous since X-rays and beta particles can be less damaging to the semiconductor material. Care must also be taken to ensure that the risk of radiation exposure to the users of microbatteries is minimised, and as

such the use of softer X-rays and beta particles is preferred compared with harder X-ray and γ-rays for that reason. Prototype temperature tolerant X-ray photovoltaic cells have also been reported using GaAs [11], $Al_{0.2}Ga_{0.8}As$ [15], and $In_{0.5}Ga_{0.5}P$ as converter materials [17]. The GaAs [55]Fe X-ray photovoltaic cell presented an open circuit voltage and maximum output power as high as 0.3 V and 1 pW, respectively, at -20 [11]. The $Al_{0.2}Ga_{0.8}As$ [55]Fe X-ray photovoltaic microbattery (two cells design) had an open circuit voltage of 0.2 V and a maximum output power of 0.04 pW at -20 °C for the best performing cell [15]. The poor results obtained for the $Al_{0.2}Ga_{0.8}As$ microbattery system were possibly caused by polarization problems due to the presence of traps in the $Al_{0.2}Ga_{0.8}As$ structure [15]. An open circuit voltage of 0.82 V and a maximum output power of 2.5 pW were instead reported for an $In_{0.5}Ga_{0.5}P$ [55]Fe X-ray photovoltaic cell at -20 °C [17]. GaAs [12, 13] and $In_{0.5}Ga_{0.5}P$ [18] photodiodes have also played a crucial role in the development of temperature tolerant betavoltaic cells. [63]Ni-GaAs and [147]Pm-GaAs microbatteries [13] have shown an open circuit voltage sensitivities of -5.30 mVK^{-1} and -4.90 mVK^{-1} in the temperature range 223.15 K to 303.15 K, respectively. An open circuit voltage sensitivity of 3.2 $mV°C^{-1}$ was also found for a [63]Ni-GaAs cell [12] between 70 °C and -20 °C; an open circuit voltage and a maximum output power as high as 0.23 V and 1.8 pW, respectively, were obtained at -20 °C. A temperature tolerant $In_{0.5}Ga_{0.5}P$ cell [18] instead has shown an open circuit voltage of 0.69 V and a maximum output power of 0.92 pW at its best operating temperature (-20 °C).

In this paper, two 400 μm diameter $Al_{0.52}In_{0.48}P$ p^+-i-n^+ mesa photodiodes with 6 μm thick i layers were characterised for their performance as converter detectors in both an [55]Fe X-ray photovoltaic microbattery and in an [63]Ni betavoltaic microbattery at temperatures from 140 °C to -20 °C. The devices are the thickest $Al_{0.52}In_{0.48}P$ layers (by a factor of 3) grown by metalorganic vapour phase epitaxy (MOVPE) so far reported in the literature. The dependence of saturation current, short circuit current, open circuit voltage, maximum output power, fill factor, and conversion efficiency as a function of temperature were studied. The highest open circuit voltage and maximum output power were found when the devices were cooled to -20 °C: values of 1.13 V and 1.44 pW, respectively, were obtained for the X-ray cell with the highest performances; whilst values of 0.47 V pA and 0.18 pW, respectively, were found for the best betavoltaic cell.

2. MATERIAL AND METHODS

2.1. Detector structure and X-ray source

The $Al_{0.52}In_{0.48}P$ structure was grown by MOVPE on an n^+ GaAs substrate. It consisted of a 0.1 μm n^+ doped layer (Si, 1×10^{19} cm^{-3}), followed by a 6 μm intrinsic layer and then a 0.2 μm p^+ doped

3

layer (Zn, 1×10^{19} cm^{-3}). A top 0.01 μm p$^+$ GaAs layer (Zn, 1×10^{19} cm^{-3}) was also included to facilitate deposition of a top Ohmic contact. Mesa diodes with diameter of 400 μm were fabricated by using standard photolithography and wet chemical etching (1:1:1 K_2:Cr_2O_7:HBr:CH_3COOHO etch, followed by finishing etch 1:8:80 H_2SO_4:H_2O_2:H_2O). A top Ohmic contact (Ti/Au, 20 nm/200 nm), covering 33% of the device surface, was deposited on top of the p$^+$ GaAs layer; whilst a rear Ohmic contact (InGe/Au, 20 nm/200 nm) was deposited onto the rear of the n$^+$ GaAs substrate. No passivation layer was applied. A total of two $Al_{0.52}In_{0.48}P$ devices (on the same die) were characterised for their X-ray voltaic and betavoltaic performances. For such measurements, a 182 MBq ^{55}Fe radioisotope X-ray source (Mn Kα = 5.9 keV, Mn Kβ = 6.49 keV) (active surface area of 6 mm in diameter) and a 185 MBq ^{63}Ni radioisotope beta source (end point energy 66 keV) (active surface area 7 mm × 7 mm) were placed 3 mm away from the detectors' top surfaces. The ^{55}Fe radioisotope X-ray source had a 0.25 mm Be window and the ^{63}Ni radioisotope beta source had a 1 μm thick inactive Ni overlayer on the active ^{63}Ni in order to meet the local radiation rules of our laboratory.

3. RESULTS

3.1. Dark Characterisation

Using a TAS Micro MT climatic cabinet and a Keithley 6487 picoammeter/voltage source, the electrical properties of the $Al_{0.52}In_{0.48}P$ photodiodes were first investigated in dark condition across the temperature range 140 °C to -20 °C. The photodiodes were forward biased between 0 V and 1.6 V in 0.01 V increments. A dry nitrogen atmosphere was created inside the climatic cabinet to reduce any humidity effects. An example of typical current as a function of forward voltage characteristic at different temperatures is presented in Figure 1 for D2; for clarity only every other temperature is shown. Similar results were obtained for D1. The decreased dark current through the device, observed when the temperature was decreased from 140 °C to -20 °C, was due to the lower thermal energy available at lower temperatures.

4
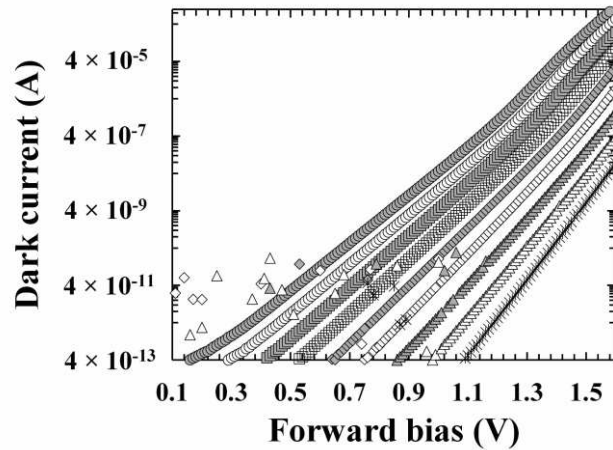
Figure 1. Dark currents as a function of applied forward bias for the $Al_{0.52}In_{0.48}P$ device, D2. The temperatures plotted were 140 °C (grey circles), 120 °C (white circles), 100 °C (grey squares), 80 °C (white squares), 60 °C (grey rhombuses), 40 °C (white rhombuses), 20 °C (grey triangles), 0 °C (empty triangles), and -20 °C (stars).

The saturation current, I_0, and the ideality factor, n, of the photodiode were extracted on the basis of the linear region of the semi-logarithm dark current as a function of forward bias. The measured saturation current and the calculated ideality factor as functions of temperature for D2 are shown in Figure 2a and Figure 2b, respectively. Similar results were obtained for D1.
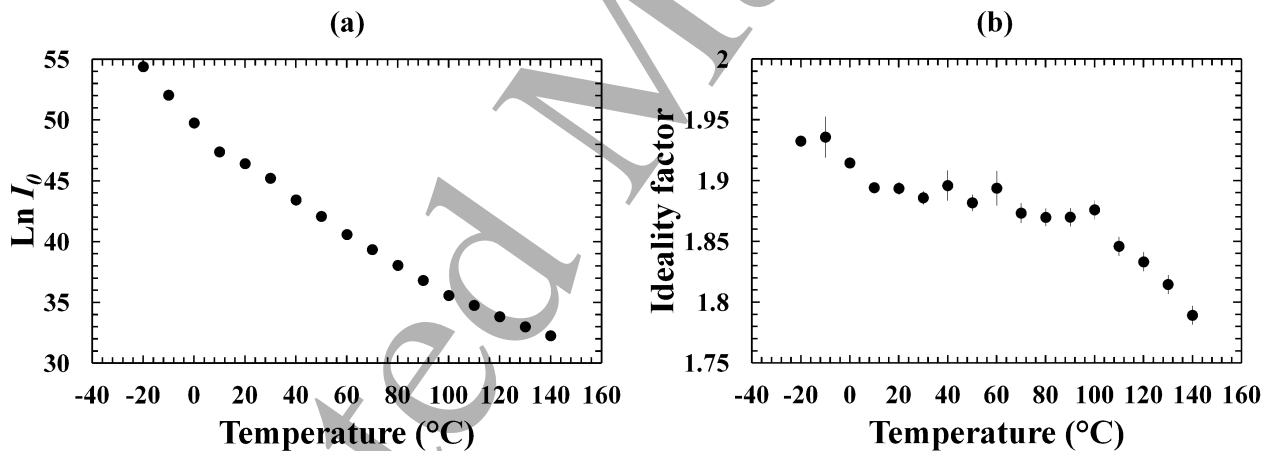
Figure 2. (a) The natural logarithm of the saturation current as a function of temperature for the $Al_{0.52}In_{0.48}P$ device, D1. (b) The ideality factor as a function of temperature for the $Al_{0.52}In_{0.48}P$ device, D1.

As expected, the natural logarithm of the saturation current increased at decreased temperatures [7]; over the temperature range 140 °C to -20 °C, an increase of 22.36 ± 0.12 (corresponding to an increase in saturation current, I_0, of 1.1 fA) was obtained for D1 and an increase of 22.13 ± 0.09 (corresponding to an increase in saturation current, I_0, of 1.0 fA) was found for D2. The results presented here were slightly lower than those reported for a 2 μm i layer $Al_{0.52}In_{0.48}P$ device, 23.13 ± 0.19, in the same range of temperatures [7].

The ideality factor for D1 was 1.797 ± 0.008 at 140 °C and it increased to 1.923 ± 0.006 at -20 °C; for D2 it was 1.789 ± 0.008 at 140 °C and it increased to 1.932 ± 0.003 at -20 °C. An ideality factor close to 2, as was found here at all temperatures studied, indicates that generation and recombination in the $Al_{0.52}In_{0.48}P$ devices were significant. The higher contribution of the diffusion current at higher temperatures possibly caused the slight decrease in ideality factor observed at 140 °C [24]. Other GaAs and AlInP photodiodes present similar dependence between ideality factor and temperature [25, 7]. The previously reported 2 μm i layer $Al_{0.52}In_{0.48}P$ device had ideality factors of 1.561 ± 0.003 and 1.682 ± 0.011 at 140 °C and -20 °C, respectively [7]; such results are lower than those reported here indicating that generation-recombination mechanism (possibly due to the higher absolute number of traps in the structure) is more significant for the 6 μm i layer $Al_{0.52}In_{0.48}P$ than it was in for the 2 μm i layer $Al_{0.52}In_{0.48}P$ photodiode [7].

3.2. X-ray photovoltaic cells

The electrical properties of the $Al_{0.52}In_{0.48}P$ photodiodes were then investigated under the illumination of the ^{55}Fe radioisotope X-ray source; the photodiodes and the ^{55}Fe radioisotope X-ray source were installed in a TAS Micro MT climatic cabinet for temperature control, data were taken at temperatures from 140 °C to -20 °C in 10 °C steps. Measurements of the devices' currents as functions of forward bias were made from 0 V to 1.6 V, with an increment step size of 0.01 V. Dry nitrogen was constantly flowed into the climatic cabinet to reduce any humidity effects. The short circuit current (I_{sc}) and open circuit voltage (V_{oc}) for both cells were measured at different temperatures; the maximum output power (P_{max}), fill factor (FF), and conversion efficiency (η) were calculated as follows [24]:

$$P_{max} = V_m I_m, \tag{1}$$

$$FF = \frac{V_m I_m}{V_{oc} I_{sc}}, \tag{2}$$

$$\eta = \frac{P_{max}}{P_i}, \tag{3}$$

where V_m and I_m are, respectively, the voltage and the current corresponding to the maximum experimental output power, and P_i is the expected incident power on the detector. The expected incident power on each of the X-ray voltaic cells was estimated by,

6

$$P_i = \frac{A}{2}\frac{A_{AlInP}}{A_{Fe}}(Em_{K\alpha}T_{K\alpha}5900 + Em_{K\beta}T_{K\beta}6490), \tag{4}$$

where $A/2$ was half of the activity of the ^{55}Fe radioisotope X-ray source (half of the X-ray photons did not contribute to the electrical power since they were emitted upwards and lost), A_{AlInP} was the area of the $Al_{0.52}In_{0.48}P$ device (0.13 mm^2), A_{Fe} was the active area of the ^{55}Fe radioisotope X-ray source (28.27 mm^2), $Em_{K\alpha}$ and $Em_{K\beta}$ were the emission probabilities of Mn Kα and Mn Kβ X-rays from the ^{55}Fe radioisotope X-ray source (0.245 and 0.0338, respectively [26]), $T_{K\alpha}$ and $T_{K\beta}$ were the transmission probabilities of Mn Kα and Mn Kβ X-rays through the 0.25 mm radioisotope X-ray source's Be window (0.576 and 0.667, respectively [27]). An incident power (P_i) of 64 pW was expected on each photodiode.

The temperature dependence of the illuminated current characteristics as a function of forward bias for one of the ^{55}Fe X-ray photovoltaic $Al_{0.52}In_{0.48}P$ cell, D2, is shown in Figure 3; similar results were obtained for D1.
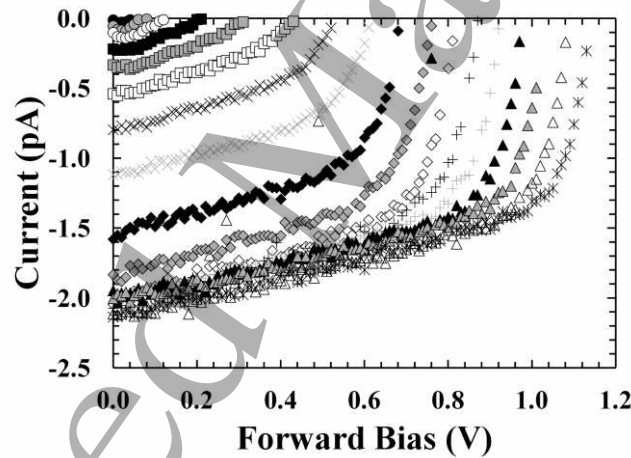
Figure 3. Illuminated current characteristics as a function of applied forward bias for ^{55}Fe X-ray photovoltaic $Al_{0.52}In_{0.48}P$ cell, D2. The temperatures analysed were 140 °C (black circles), 130 °C (grey circles), 120° C (white circles), 110 °C (black squares), 100 °C (grey squares), 90 °C (white squares), 80 °C (black crosses), 70 °C (grey crosses), 60 °C (black rhombuses), 50 °C (grey rhombuses), 40 °C (white rhombuses), 30°C (black plus signs), 20 °C (grey plus signs), 10 °C (black triangles), 0 °C (grey triangles), -10 °C (white triangles), and -20 °C (stars).

The values, extrapolated from Figure 3, of the short circuit current (I_{sc}) and open circuit voltage (V_{oc}) as a function of temperature for D2 are presented in Figure 4a and Figure 4b, respectively; similar dependences were found for D1.

7
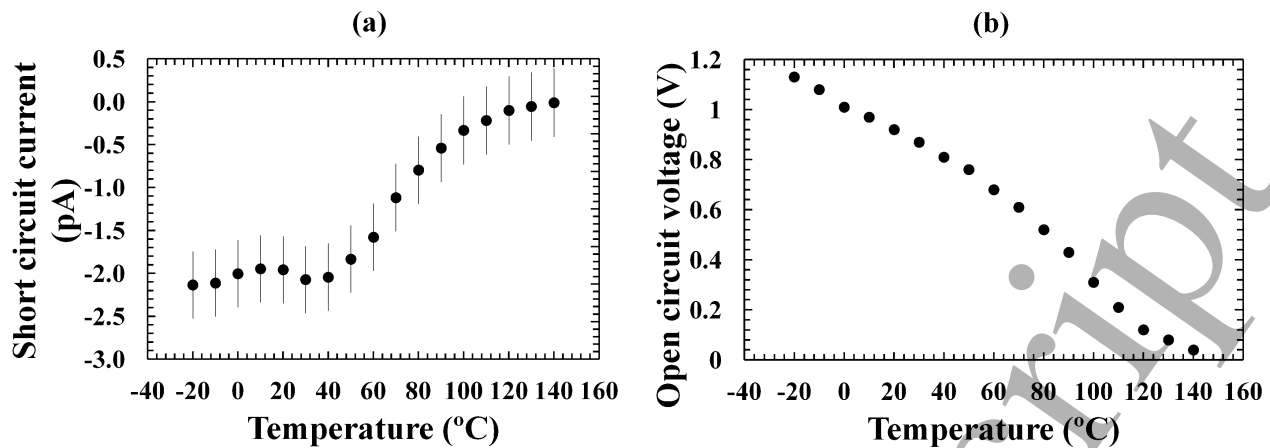
Figure 4. (a) Short circuit current as a function of temperature for the [55]Fe X-ray photovoltaic $Al_{0.52}In_{0.48}P$ cell, D2. (b) Open circuit voltage as a function of temperature for the [55]Fe X-ray photovoltaic $Al_{0.52}In_{0.48}P$ cell D2.

The short circuit current magnitude increased when the temperature was reduced from 140 °C to 50 °C, whilst it remained stable ($\approx$2.5 pA for D1 and $\approx$2 pA for D2, respectively) at temperatures between 40 °C and -20 °C. The short circuit current is dependent on the number of carriers generated upon X-ray photon absorption and the carrier diffusion lengths; while the former decreased at low temperature because of the higher electron-hole pair creation energy, the later increased at low temperature because of the lower thermal (phonon) scattering. For both the cells, the experimental results showed that the thermal scattering mechanism was predominant in the temperature range 140 °C to 50 °C, whilst it was possibly compensated by the decrease in the number of carrier generated in the temperature range 40 °C to -20 °C. A flat trend in the short circuit current was instead observed for a [55]Fe X-ray photovoltaic 2 μm i layer $Al_{0.52}In_{0.48}P$ cell between 160 °C to -20 °C [7]. At -20 °C, the short circuit current observed here was more than 2 times bigger than that observed for the 2 μm i layer $Al_{0.52}In_{0.48}P$ cell.

An open circuit voltage (V_{oc}) as high as 1.13 V was observed in both $Al_{0.52}In_{0.48}P$ X-ray photovoltaic cells at -20 °C. The V_{oc} is linearly dependent on the temperature with a gradient of (0.00554 ± 0.00010) V°C^{-1} between 40 °C and -20 °C and a gradient of (0.00843 ± 0.00014) V°C^{-1} between 130 °C and 50 °C for D1. Similar results were found for D2, gradients of (0.00525 ± 0.00013) V°C^{-1} and (0.0090 ± 0.0003) V°C^{-1} were measured in the temperature ranges 40 °C to -20 °C, and 130 °C to 50 °C, respectively. The steeper gradient obtained, in both $Al_{0.52}In_{0.48}P$ X-ray photovoltaic cells, between 130 °C and 50 °C, may be explained by the increased thermal scattering mechanism which decreased the carrier mobility (lower photocurrent) resulting in a more rapid decrease of V_{oc}. The gradients obtained between 40 °C and -20 °C were similar to those reported for the 2 μm i layer $Al_{0.52}In_{0.48}P$ [55]Fe radioisotope microbatteries, (0.00460 ± 0.00003) V°C^{-1} [7]

8

The high V_{oc} values found here are due to the large bandgap energy of $Al_{0.52}In_{0.48}P$ (at room temperature, 2.31 eV [4]). To obtain a large V_{oc}, a large bandgap (E_G) is required; this is because the V_{oc} increases logarithmically with decreasing saturation current (I_0), and I_0 decreases exponentially with E_G [24]. As expected, the $Al_{0.52}In_{0.48}P$ cells have higher V_{oc} values than those observed in X-ray voltaic cells where GaAs (bandgap at room temperature of 1.42 eV [28]) or $In_{0.5}Ga_{0.5}P$ (bandgap at room temperature of 1.9 eV [29]) devices are used as converter layers [11, 17]. Higher open circuit voltage values were also observed here compared to a 2 μm i layer $Al_{0.52}In_{0.48}P$ [55]Fe cells due to the larger number of carriers generated in the 6 μm (cf. 2 μm) i layer cells. Both the 2 μm i layer and 6 μm i layer $Al_{0.52}In_{0.48}P$ structures had similar saturation currents [7].

The output power (P) extracted from one of the [55]Fe X-ray photovoltaic $Al_{0.52}In_{0.48}P$ cell (D2) is shown in Figure 5a; the output power increased to a maximum (P_{max}), corresponding to a voltage of V_m and a current of I_m, and then decreased at increased forward bias. Figure 5b shows a zoom of Figure 5a so as to illustrate the results observed at 140 °C, 130 °C, and 120 °C.
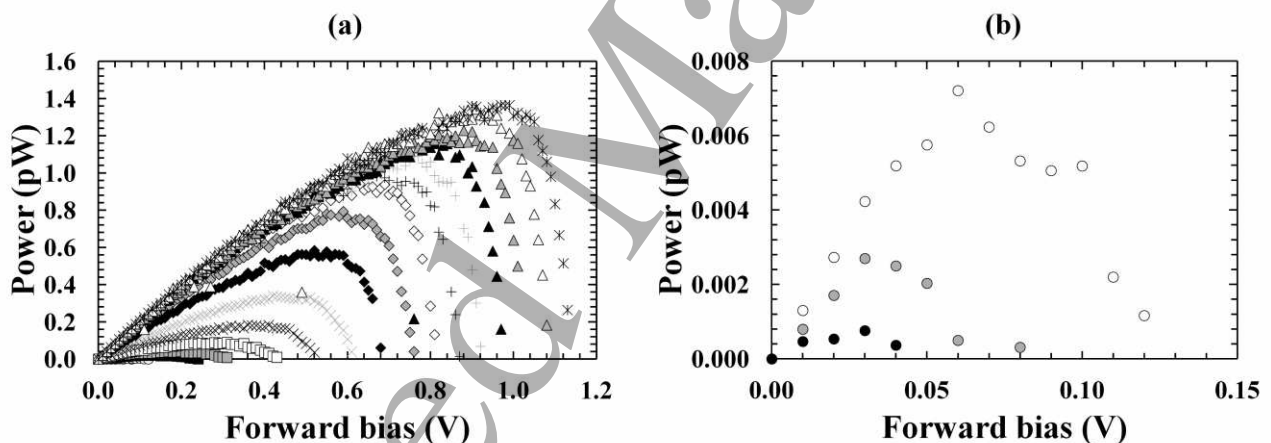
Figure 5. (a) Output power as a function of applied forward bias for the [55]Fe X-ray photovoltaic $Al_{0.52}In_{0.48}P$ cell, D2, at different temperatures. The temperatures analysed were 140 °C (black circles), 130 °C (grey circles), 120 °C (white circles), 110 °C (black squares), 100 °C (grey squares), 90 °C (white squares), 80 °C (black crosses), 70 °C (grey crosses), 60 °C (black rhombuses), 50 °C (grey rhombuses), 40 °C (white rhombuses), 30 °C (black plus signs), 20 °C (grey plus signs), 10 °C (black triangles), 0 °C (grey triangles), -10 °C (white triangles) and -20 °C (stars). (b) Zoom showing in detail the output power obtained at 140 °C (black circles), 130 °C (grey circles), and 120 °C (white circles).

The maximum output power (P_{max}) was found using equation 1; its relationship with temperature for D2 is shown in Figure 6a. Similar results were obtained for D1. Because of the linear dependence of P_{max} on V_{oc}, increased P_{max} values were obtained at decreased temperatures [24]. The different behaviour observed at temperatures below 50 °C was in accordance with the results found for V_{oc} in

the same temperature range. The fill factor is the measure of the sharpness of the current as a function of forward bias characteristics. For each $Al_{0.52}In_{0.48}P$ cell, the fill factor (*FF*) was calculated using equation 2. Figure 6b shows *FF* as a function of temperature for D2: the fill factor decreased from 140 °C to 100 °C, then slightly increased from 100 °C to 60 °C and saturated to a value of ≈0.5 for temperatures lower than 60 °C. Similar results were obtained for D1.
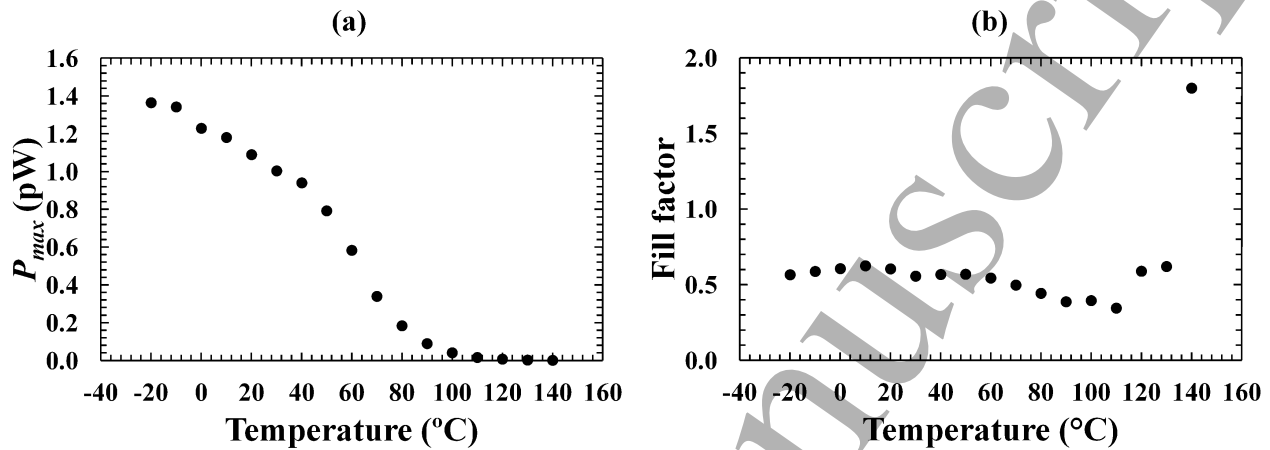

Figure 6. (a) Maximum output power as a function of temperature for the [55]Fe X-ray photovoltaic $Al_{0.52}In_{0.48}P$ cell, D2. (b) Fill factor as a function of temperature for the [55]Fe X-ray photovoltaic $Al_{0.52}In_{0.48}P$ cell, D2.

The conversion efficiency (η) was estimated using equation 3; its dependence on temperature for D2 is presented in Figure 7. Similar results were obtained for D1. The conversion efficiency increased at decreased temperatures, it reached its maximum value of 2.2% for D1 and 2.1% for D2 at -20 °C. Dividing the experimental output power by the power actually absorbed by each device, internal conversion efficiencies of 25% and 24% were found at -20 °C for D1 and D2, respectively. In the calculation of the power actually absorbed, the device quantum efficiency (50% at 5.9 keV and 42% at 6.49 keV) and the $Al_{0.52}In_{0.48}P$ electron hole pair creation energy at each specific temperature [30] were used. The device quantum efficiency (*QE*) was calculated using the Beer-Lambert law and assuming complete charge collection in the $Al_{0.52}In_{0.48}P$ i layer. The linear attenuation coefficients used in the *QE* calculations were 0.13 μm^{-1} and 0.10 μm^{-1} at 5.9 keV and 6.49 keV, respectively [27, 31]; these values are higher than for many other semiconductors such as Si, GaAs, and AlGaAs [27, 31].
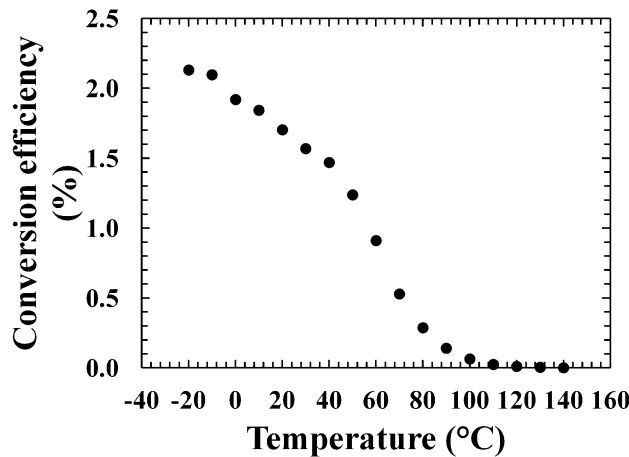
10

Figure 7. Conversion efficiency (η) as a function of temperature for the $Al_{0.52}In_{0.48}P$ [55]Fe X-ray photovoltaic cell.

The highest maximum output power was observed at -20 °C for both the X-ray voltaic cells; values of 1.44 pW and 1.36 pW were obtained for D1 and D2, respectively. At the same temperature, a 10 μm i layer GaAs [55]Fe X-ray photovoltaic cell shown an output power of 1 pW [13]; the decreased output power extracted from the GaAs converter cell is due to the higher X-ray attenuation coefficients of $Al_{0.52}In_{0.48}P$ with respect to GaAs. A 5 μm i layer $In_{0.5}Ga_{0.5}P$ [55]Fe X-ray photovoltaic cell had instead an output power of 1.5 pW at -20 °C [18]; the better performance of such a cell was a consequence of the higher X-ray attenuation coefficients of $In_{0.5}Ga_{0.5}P$ with respect to $Al_{0.52}In_{0.48}P$.

The increased output power reported here with respect to the earlier $Al_{0.52}In_{0.48}P$ device [7] is due to the new $Al_{0.52}In_{0.48}P$ detectors being thicker; the i layer of the $Al_{0.52}In_{0.48}P$ devices characterised here was 3 times thicker than that of the photodiodes used in ref. [7]. A further increase of the $Al_{0.52}In_{0.48}P$ i layer thickness may improve the number of X-ray photons absorbed in the detector and consequently increased the extracted output power. This improvement is expected from quantum efficiency calculations based on absorption of radiation in the active region of the structure (using the Beer-Lamber law). Deviation from ideal material qualities in thicker structures may result in the optimal real-world structure thickness being thinner than this, even if complete absorption is not possible within that thinner structure. An advantage of the reported $Al_{0.52}In_{0.48}P$ [55]Fe radioisotope microbattery is that the output powers of the two 400 μm diameter $Al_{0.52}In_{0.48}P$ X-ray photovoltaic cells could be combined, resulting in a combined output power of 2.8 pW at -20 °C; a real word microbattery would necessarily use many cells combined and/or cells of larger area. Table I shows the maximum output powers at some significant temperatures for both of the 6 μm i layer $Al_{0.52}In_{0.48}P$ detectors analysed.

Table I. Maximum output powers from the $Al_{0.52}In_{0.48}P$ X-ray photovoltaic cells at particular temperatures.

Temperature (°C)	Maximum Power D1 (pW)	Maximum Power D2 (pW)
-20	1.435	1.364
20	1.083	1.090
60	0.565	0.584
100	0.041	0.041
140	0.005	0.001

3.3. Betavoltaic cells

The [55]Fe radioisotope X-ray source was then substituted with the [63]Ni radioisotope beta source, the change in the electrical performance of the $Al_{0.52}In_{0.48}P$ photodiodes under this type of radiation were studied using the same techniques as described above. Although temperatures up to 140 °C were reached during the experiment, betavoltaic characteristics were only observed below 110 °C in both photodiodes. Figure 8 shows the illuminated currents recorded between 110 °C and -20 °C from D2; similar characteristics were found for D1.
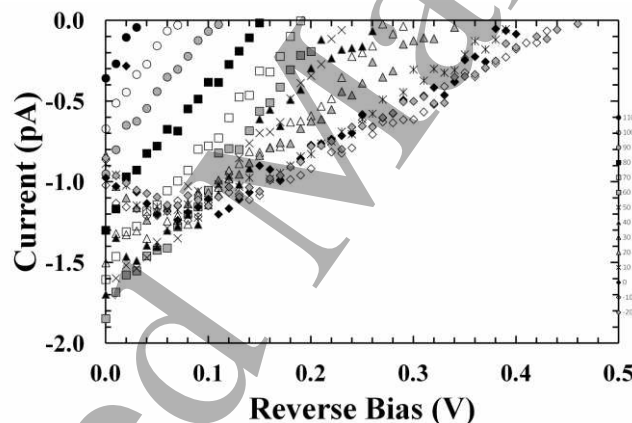
Figure 8. Illuminated current characteristics as a function of applied forward bias for [63]Ni betavoltaic $Al_{0.52}In_{0.48}P$ cell, D2. The temperatures analysed were 110 °C (black circles), 100 °C (white circles), 90° C (grey circles), 80 °C (black squares), 70 °C (white squares), 60 °C (grey squares), 50 °C (crosses), 40 °C (black triangles), 30 °C (white triangles), 20 °C (grey triangles), 10 °C (stars), 0 °C (black rhombuses), -10 °C (white rhombuses), -20 °C (grey rhombuses).

Short circuit current (I_{sc}) and open circuit voltage (V_{oc}) values were extracted from Figure 8, their values were lower than those observed during the X-ray photovoltaic experiment for both the betavoltaic cells; Figure 9a and 9b show the results found for D2. Similar dependences were obtained for D1.

12

Figure 9. (a) Short circuit current as a function of temperature for the ^{63}Ni betavoltaic $Al_{0.52}In_{0.48}P$ cell, D2. (b) Open circuit voltage as a function of temperature for the ^{63}Ni betavoltaic $Al_{0.52}In_{0.48}P$ $Al_{0.52}In_{0.48}P$ cell D2.
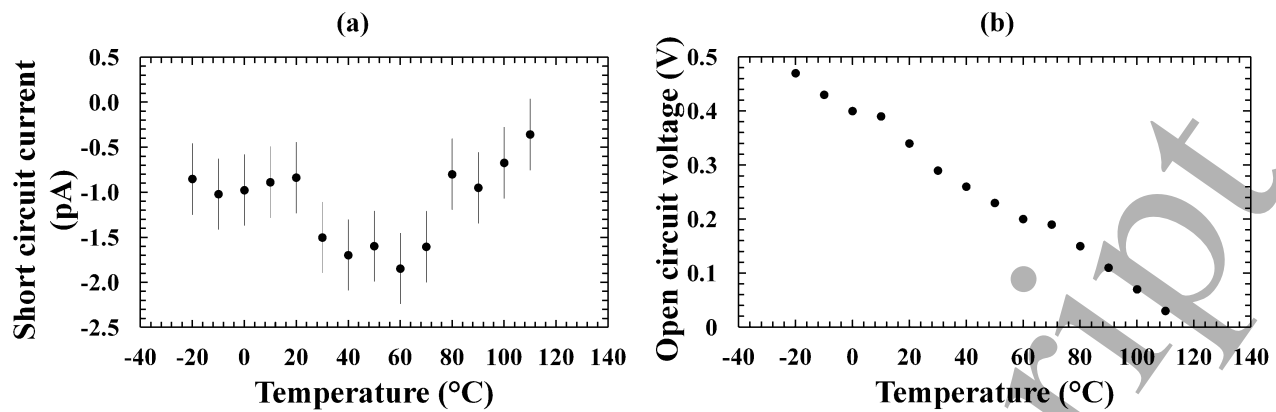
The magnitude of the short circuit current increased from 110 °C to 60 °C, and remained stable (≈1.7 pA for D1 and ≈1.8 pA for D2, respectively) from 60 °C to 30 °C. Such behaviour was similar to that previously found in the X-ray photovoltaic experiment, although the value at each particular temperature was lower than that under the illumination of the ^{55}Fe radioisotope X-ray source. Unexpectedly, at temperatures below 30 °C, the short circuit current decreased to ≈1 pA in both photodiodes. The mechanism that caused such decrease is unclear, it may be due to the presence of trapping centres whose probability of releasing a trapped carrier decreased at low temperatures. Previously, a decrease in short circuit current magnitude has also been observed for a ^{63}Ni betavoltaic $Al_{0.52}In_{0.48}P$ (2 μm i layer) cell [8] at the same temperatures; at -20 °C, the short circuit current for the 2 μm i layer $Al_{0.52}In_{0.48}P$ cell was more than 2 times bigger than that observed here. Higher short circuit currents were also observed for the GaAs [12] (27 pA) and $In_{0.5}Ga_{0.5}P$ [18] (4.5 pA) betavoltaic cells at -20 °C.

The $Al_{0.52}In_{0.48}P$ cells D1 and D2 presented open circuit voltages (V_{oc}) of 0.34 V and 0.47 at -20 °C, respectively. Such values are much lower than the ones obtained previously for the same photodiodes operating in X-ray photovoltaic mode. The decreased short circuit current observed for the betavoltaic cells (particularly at low temperatures) with respect to the X-ray photovoltaic cells, decreased the open circuit voltage in accordance with equation 5. The short circuit current results are surprising since the expected number of carriers generated under the illumination of the X-ray source (4×10^7 at -20 °C) was lower than the number of carriers generated under the illumination of the beta source (17×10^7 at -20 °C). The different interaction mechanism between X-rays or beta particles and the semiconductor also possibly contributed to the decrease in open circuit voltage. Each 5.9 keV and 6.49 keV X-ray can be considered, as an approximation, to be

13

absorbed each in one location (the authors acknowledge the non-zero ranges of the photoelectron and detector's self-fluorescence X-ray upon interaction but consider these to be short for the present case). In contrast, each beta particle loses energy along its track through the semiconductor. This can lead to localised reductions in the electric field strength (reduced resistivity) along these tracks. An excessively large number of charge carriers created in the semiconductor (regardless of whether created along tracks or uniformly in the device) can also cause a reduction in the resistivity of the device [32]. These effects may be the origin of the lower observed open circuit voltage values (V_{oc}).

$$V_{oc} = \frac{kT}{q} ln\left(\frac{I_{sc}}{I_0} + 1\right) \tag{5}$$

where k is the Boltzmann constant, T the temperature, q the charge, I_{sc} the short circuit current, and I_0 the saturation current. The open circuit voltages obtained here were also lower than those obtained for a ^{63}Ni betavoltaic $Al_{0.52}In_{0.48}P$ (2 μm i layer) cell [8]: that cell had a $V_{oc} = 0.52$ V at -20 °C. This is mainly a consequence of the lower short circuit currents observed for the 6 μm i layer $Al_{0.52}In_{0.48}P$ structure with respect to the 2 μm i layer $Al_{0.52}In_{0.48}P$ device. The betavoltaic results reported here are important since they show that it is not always the case that a thicker absorption region and greater numbers of created charge carriers result in better betavoltaic cell performances; other mechanisms can also influence the betavoltaic system, and these mechanisms need to be considered in order to achieve the best betavoltaic cell design. The previously reported GaAs [12] and $In_{0.5}Ga_{0.5}P$ [18] betavoltaic cells presented lower (0.2 V) and higher (0.69 V) open circuit voltage values, respectively, than those found for the 6 μm i layer $Al_{0.52}In_{0.48}P$ betavoltaic cells.

The output power (P) as a function of forward bias for the ^{63}Ni betavoltaic $Al_{0.52}In_{0.48}P$ cell (D2) is shown in Figure 10; similar output powers were extracted from D1.

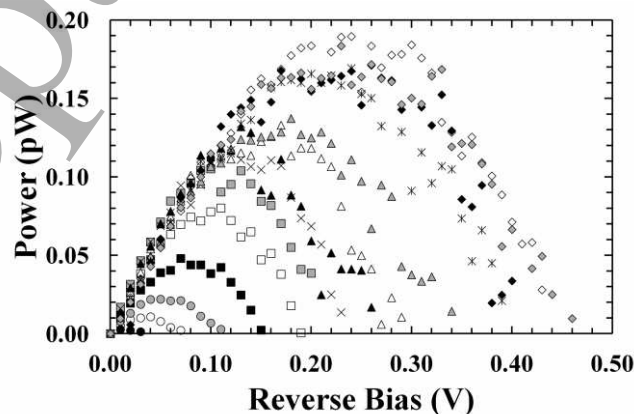
Figure 10. Output power as a function of applied forward bias for the ^{63}Ni betavoltaic $Al_{0.52}In_{0.48}P$ cell, D2, at different temperatures. The temperatures analysed were 110 °C (black circles), 100 °C

14

(white circles), 90° C (grey circles), 80 °C (black squares), 70 °C (white squares), 60 °C (grey squares), 50 °C (crosses), 40 °C (black triangles), 30 °C (white triangles), 20 °C (grey triangles), 10 °C (stars), 0 °C (black rhombuses), -10 °C (white rhombuses), -20 °C (grey rhombuses).

Equation 1 was used to calculate the maximum output power (P_{max}) extracted from the betavoltaic cells at different temperatures, Figure 11a shows the results obtained for D2. Similar dependence of P_{max} from the temperature was found for D1. The results reflected the linear relationship of P_{max} on V_{oc}; the lower maximum output power for the 6 μm i layer $Al_{0.52}In_{0.48}P$ structure with respect to the 2 μm i layer $Al_{0.52}In_{0.48}P$ device [8] was a consequence of the lower open circuit voltage of the former cell. The fill factor (FF) was found using equation 2, Figure 11b shows FF as a function of temperature for D2. The behaviour was similar to that found for the X-ray photovoltaic cell: the fill factor decreased from 110 °C to 90 °C, then remained quite stable with an increased at low temperatures.
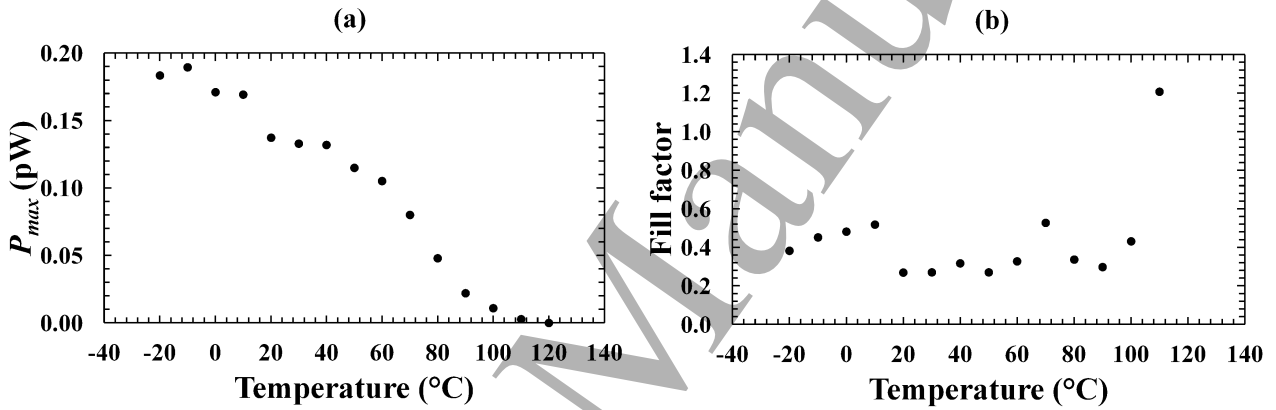

Figure 11. (a) Maximum output power as a function of temperature for the [63]Ni betavoltaic $Al_{0.52}In_{0.48}P$ cell, D2. (b) Fill factor as a function of temperature for the [63]Ni betavoltaic $Al_{0.52}In_{0.48}P$ cell, D2.

Equation 3 was used to evaluate the conversion efficiency (η); the expected incident power on each betavoltaic cell was estimated by,

$$P_i = \sum_{i=0}^{endpoint=66} \frac{A}{2} \frac{A_{AlInP}}{A_{Ni}} Em_i T_i i \tag{6}$$

where $A/2$ was half of the activity of the [63]Ni radioactive source (taking into account self-absorption mechanisms; only half of the beta electrons were considered because the other half were emitted upwards and lost), A_{AlInP} was the area of the $Al_{0.52}In_{0.48}P$ device (0.13 mm^2), A_{Ni} was the active area of the [63]Ni radioisotope beta source (49 mm^2), Em_i was the emission probability of an electron of energy i [33], T_i was the transmission probability of an electron of energy i through the Ni overlayer and dry nitrogen. Monte Carlo computer modelling package CASINO (version 2.48) [34, 35] was

used to simulate the attenuations of the beta particles through the 1 μm thick inactive Ni overlayer and the 3 mm of dry nitrogen. Self-absorption mechanisms within the ^{63}Ni beta source were taken into account in the calculations, this reduced the source activity from 185 MBq to 136 MBq [36] if a specific activity of 13 mCimg^{-1} was considered (according the source supplier specifications). An incident power (P_i) of 287 pW was estimated on each photodiode. The temperature dependence of the conversion efficiency for D2 is shown in Figure 12; the dependence for D1 was similarly obtained. In accordance with the X-ray photovoltaic cells, the conversion efficiency had its maximum value at -20 °C (0.04% for D1 and 0.06% for D2), whilst it decreased when the temperature increased.
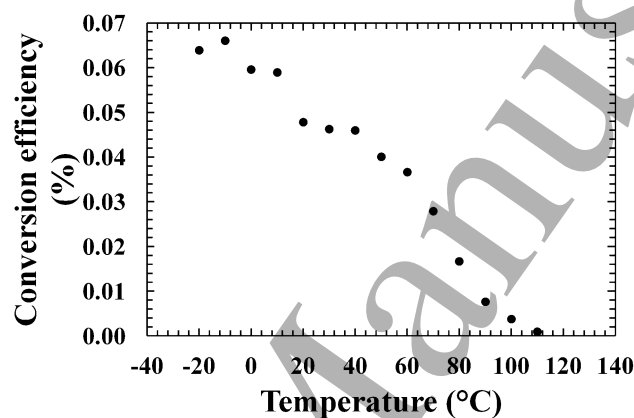

Figure 12. Conversion efficiency (η) as a function of temperature for the Al$_{0.52}$In$_{0.48}$P ^{63}Ni betavoltaic cell.

Dividing the experimental output power by the power actually absorbed by each device, internal conversion efficiencies of 0.5% and 0.7% were found at -20 °C for D1 and D2, respectively. In order to calculate the power actually absorbed, the Al$_{0.52}$In$_{0.48}$P electron hole pair creation energy at each specific temperature [30] was used. It was also necessary to evaluate the cell quantum efficiencies (*QE*): the computer model package CASINO was used to estimate the percentage of the energy of the electron absorbed within the Al$_{0.52}$In$_{0.48}$P i layer with respect to the energy incident at the photodiode face (*QE*) as a function of electrons energies (1-66 keV). Figure 13 shows the simulated quantum efficiency.
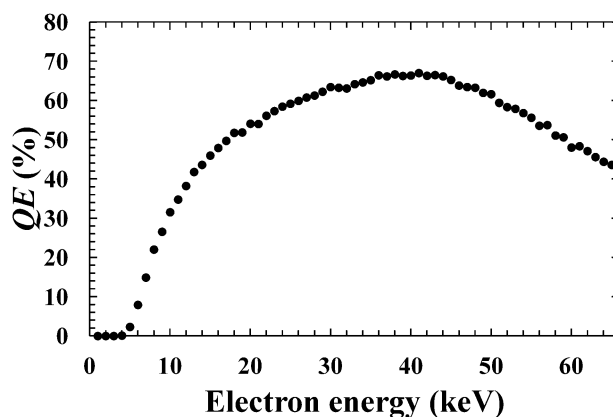
Figure 13. *QE* of the $Al_{0.52}In_{0.48}P$ structure as a function of electron energy as determined by Monte Carlo modelling

At -20 °C, maximum output powers as high as 0.13 pW and 0.18 pW were extracted from D1 and D2, respectively. At the same temperature, a 10 μm i layer GaAs cell [12], a 5 μm i layer $In_{0.5}Ga_{0.5}P$ [18], and a 2 μm i layer $Al_{0.52}In_{0.48}P$ betavoltaic cell [8] presented higher maximum output powers. Such differences in results were a direct consequence of the lower values for the product between open circuit voltage and short circuit current in the 6 μm i layer $Al_{0.52}In_{0.48}P$ betavoltaic cells with respect to cells where different converter materials were used. Combining the output powers of the two 6 μm i layer $Al_{0.52}In_{0.48}P$ betavoltaic cells, a total output power of 0.3 pW could be found at -20 °C. The maximum output powers extracted from both the 6 μm i layer $Al_{0.52}In_{0.48}P$ cells are reported in Table II.

Table II. Maximum output powers from the $Al_{0.52}In_{0.48}P$ betavoltaic cells at particular temperatures.

Temperature (°C)	Maximum Power D1 (pW)	Maximum Power D2 (pW)
-20	0.125	0.183
20	0.071	0.137
60	0.097	0.105
100	0.002	0.001

Table III shows the key performance parameters obtained for the 6 μm i layer $Al_{0.52}In_{0.48}P$ X-ray photovoltaic and betavoltaic cells compared with those previously reported 2 μm i layer $Al_{0.52}In_{0.48}P$ X-ray voltaic [7] and betavoltaic [8] cells, at -20 °C.

Table III. Key performance parameters for the current 6 μm and previous 2 μm i layer Al0.52In0.48P X-ray photovoltaic [7] and betavoltaic cells [8], at -20 °C.

	6 μm $Al_{0.52}In_{0.48}P$		2 μm $Al_{0.52}In_{0.48}P$	
	X-ray voltaic cell	Betavoltaic cell	X-ray voltaic cell	Betavoltaic cell

17

Short circuit current	2.5 pA	1.0 pA	1.2 pA	2.3 pA
Open circuit voltage	1.13 V	0.47 V	0.97 V	0.52 V
Max output power	1.44 pW	0.18 pW	0.62 pW	0.28 pW

4. CONCLUSION

In this work, a 182 MBq ^{55}Fe radioisotope X-ray source and a 185 MBq ^{63}Ni radioisotope beta source were used, in turn, to illuminate two 400 μm diameter p^+-i-n^+ (6 μm i layer) $Al_{0.52}In_{0.48}P$ unpassivated mesa photodiodes (D1 and D2). The $Al_{0.52}In_{0.48}P$ devices are the thickest $Al_{0.52}In_{0.48}P$ photodetectors reported to date for this emerging application. Optimal thicknesses of 40 μm and 25 μm of $Al0.52In0.48P$ would be needed to maximize the number of charge carriers usefully created by 55Fe X-ray and 63Ni beta particle radioisotope sources, respectively; deviation from ideal material qualities may result in the optimal real-world structure thicknesses being thinner than these. The 6 μm thick i layer was a step forward towards these thicknesses. The conversion of X-ray energy/beta energy into electrical energy was achieved using the exceptional properties of $Al_{0.52}In_{0.48}P$ as converter layer. The ^{55}Fe radioisotope $Al_{0.52}In_{0.48}P$ microbattery cells and the ^{63}Ni radioisotope $Al_{0.52}In_{0.48}P$ microbattery cells were analysed over the temperature range 140 °C to -20 °C. The electrical properties of the $Al_{0.52}In_{0.48}P$ photodiodes were firstly investigated in dark conditions to study the saturation current and the ideality factor as a function of temperature. Increases in the logarithm of saturation current and ideality factor were observed when the temperature was decreased from 140 °C to -20 °C. The electrical properties of the $Al_{0.52}In_{0.48}P$ devices were then investigated under the illumination of the ^{55}Fe radioisotope X-ray source and the ^{63}Ni radioisotope beta source. The short circuit current, the open circuit voltage, the maximum output power, the fill factor, and the conversion efficiency were studied as a function of temperature for the X-ray voltaic and betavoltaic cells. An increase in open circuit voltage, maximum power, and conversion efficiency was found when decreasing the temperature. For the X-ray photovoltaic cells, an open circuit voltage as high as 1.13 V was obtained at -20 °C for both devices; whilst a maximum output powers of 1.44 pW and 1.36 pW were extracted at -20 °C for D1 and D2, respectively. Combining such output powers a total maximum output power as high as 2.8 pW could be obtained at -20 °C. Poorer performances were instead observed for the betavoltaic cells: open circuit voltages of 0.34 V and 0.47 V and maximum output powers of 0.13 pW and 0.18 pW were found for D1 and D2, respectively, at -20 °C. A total output power of 0.3 pW could be found at -20 °C, combining the powers extracted from both cells. The different mechanisms in the beta particle-semiconductor interaction with respect to X-ray-semiconductor interaction may explain the differences in results found.

18

ACKNOWLEDGMENTS

DATA AVAILABILITY

Whilst all data from the study and the findings are contained within the paper, further requests for information may be addressed to the authors.

REFERENCES

[1] Imanishi D 2017 *Jpn. J. Appl. Phys.* **56**, 032702.

[2] Vaisman M, Mukherjee K, Masuda T, Yaung K N, Fitzgerald E A and Lee M L 2016 *IEEE J. Photovolt.* **6**, 571.

[3] Cheong J S, Ong J S, Ng J S, Krysa A B. and David J P R 2014 *IEEE J. Sel. Topics Quantum Electron.* **20**, 142.

[4] Bower K E, Barbanel Y A, Shreter Y G and Bohnert G W 2002 *Polymers, phosporors, and voltaics for radioisotope microbatteries*, CRC Press LLC, Boca Raton.

[5] Kotzar G, Freas M, Abel P, Fleischman A, Roy S, Zorman C, Moran J M and Melzak J 2002 *Biomaterials* **23**, 2737.

[6] Landis G A, Bailey S G, Clark E B, Myers M G, Piszczor M F and Murbach M S 2012 *38th IEEE Photovoltaic Specialists Conference,* PVSC (3-8 June 2012), Austin (USA), 002819.

[7] Butera S, Lioliou G, Krysa A B and Barnett A M 2016 *J. Phys. D: Appl. Phys.* **49**, 355601.

[8] Butera S, Lioliou G, Krysa A B and Barnett A M 2016 *J. Appl. Phys.* **120**, 144501.

[9] Duggirala R, Lal A and Radhakrishnan S 2010 *Radioisotope Thin-Film powered Microsystems*, Springer, New York.

[10] Chandrashekhar M, Thomas C I, Li H, Spencer M G and Lal A 2006 *Appl. Phys. Lett.* **88**, 0335061.

[11] Butera S, Lioliou G and Barnett A M 2016 *J. Appl. Phys.* **119**, 064504.

[12] Butera S, Lioliou G. and Barnett A M 2017 *Appl. Radiat. Isot.* **125**, 42.

[13] Wang G, Hu R, Wei H, Zhang H, Yang Y, Xiong X, Liu G and Luo S 2010 *Appl. Radiat. Isot.* **68**, 2214.

[14] Eiting C J, Krishnamoorthy V, Rodgers S and George T 2006 *Appl. Phys. Lett.* 88, 064101.

[15] Butera S, Whitaker M D C, Lioliou G and Barnett A M 2016 *Sci. Rep.* **6**, 38409 (2016).

[16] Deus S 2000 *28th IEEE Photovoltaic Specialists Conference,* PVSC (15-22 September 2000), Anchorage (USA), 1246.

[17] Butera S, Whitaker M D C, Krysa A B and Barnett A M 2017 *Sci. Rep.* **7**, 4981.

[18] Butera S, Whitaker M D C, Krysa A B and Barnett A M 2017. *J. Phys. D: Appl. Phys.* **50**, 345101.

[19] Cress C D, Landis B J, Raffaelle R P and Wilt D M 2006 *J. Appl. Phys.* **100**, 114519.

[20] Cabauy P, Olsen L C and Pan N 2016 *Patent US 9466401 B1*.

[21] Cheng Z, Chen X, San H, Feng Z and Liu B 2012 *J. Micromech. Microeng.* **22,** 074011.

[22] Munson C E, Gaimard Q, Merghem K, Sundaram S, Rogers D J, De Sanoit J, Voss P L, Ramdane A, Salvestrini JP and Ougazzaden A 2017 *J. Phys. D: Appl. Phys.* **51**, 035101.

[23] Delfaure C, Pomorski M, De Sanoit J, Bergonzo P and Saada 2016 *Appl. Phys. Lett.* **108**, 252105.

[24] Sze S M and Ng K K 2007 *Physics of semiconductor devices*, Third Ed., John Wiley & Sons, New Jersey.

[25] Lioliou G, Meng X, Ng J S and Barnett A M 2016 *J. Appl. Phys* **119**, 124507 (2016).

[26] Shotzig U 2000 *Appl. Radiat. Isot.* **53**, 469 (2000).

[27] Hubbell J H 1982 *Int. J. Appl. Radiat. Is.* **33**, 1269.

[28] Bertuccio G and Maiocchi D 2002 *J. Appl. Phys.* **92**, 1248.

[29] Nelson R J and Holonyak N Jr 1976 *Phys. Chem. Solids* **37**, 629.

[30] Butera S, Lioliou G, Krysa A B and Barnett A M 2017 *Nucl. Instrum. Methods Phys. Res. Sect. A* **879**, 64.

[31] Jenkins R, Gould R W and Gedcke D 1995 *Quantitative X-ray Spectrometry*, Second Ed., CRC Press, New York.

[32] Knoll G F 2010 *Radiation Detection and Measurement*, Fourth Ed., John Wiley & Sons, New Jersey.

[33] Liu Y P, Tang X B, Xu Z H, Hong L, Wang H, Liu M and Chen D 2015 *J. Radioanal. Nucl. Chem.* **304**, 517.

[34] Hovington P, Drouin D and Gauvin R 1997 *Scanning* **19**, 1.

[35] Drouin D, Hovington P and Gauvin R 1997 *Scanning* **19**, 20.

[36] Alam T R and Pierson M A 2016 *J. Energy* **3**, 11.